RSC Advances

PAPER

View Article Online
View Journal | View Issue

Cite this: *RSC Adv.*, 2024, **14**, 1195

Design and application of histidine-functionalized ZnCr-LDH nanozyme for promoting bacteria-infected wound healing

Sonya Dadakhani,[a] Gholamreza Dehghan,*[a] Alireza Khataee*[bc] and Amir Erfanparast[d]

Excessive use of antibiotics can lead to an increase in antibiotic-resistant bacteria, which makes it a serious health threat. Therefore, developing new materials with antibacterial activity, such as nanozymes, has gained considerable attention. Reactive oxygen species (ROS) produced by nanozymes have rapid and effective antibacterial efficacy. Here, histidine (His) modified ZnCr layered double hydroxide (LDH) was synthesized inspired by the natural enzyme, and the enzyme-like activity of His/ZnCr-LDH was tested using a colorimetric method. Then, we developed an acid-enhanced antibacterial method based on the high peroxidase-like activity of His/ZnCr-LDH, and its ROS-generating capability in the presence of glucose oxidase (GOx) and glucose (Glu) as a source of hydrogen peroxide (H_2O_2). Gluconic acid (GA), the main product of the GOx reaction, provides an acidic environment and promotes ROS generation. The mentioned strategy shows high antibacterial activity at a low minimum inhibitory concentration (MIC) which represents the potential of His/ZnCr-LDH for effective bacterial elimination (3.5 μg mL^{-1} for *S. aureus* and 6 μg mL^{-1} for *E. coli*). In addition, animal experiments illustrated that the His/ZnCr-LDH can successfully boost the curing of infected wounds. The outcomes indicate that amino acid modified LDHs offer a new strategy for effective bacterial removal in different medical applications.

Received 29th October 2023
Accepted 4th December 2023

DOI: 10.1039/d3ra07364e

rsc.li/rsc-advances

1. Introduction

Enzymes are usually globular proteins of biological origin that can catalyze reactions under mild conditions (aqueous solution at ambient temperature and pressure, *etc.*) and are widely utilized in medical, industrial, and various biological fields due to their high stereoselectivity and substrate specificity.[1,2] Nevertheless, they suffer from some weak points, including instability, time-consuming procedures, inactivation through non-optimal conditions, high price, easy denaturation, and difficulty in their preparation, purification, and storage in biology and nanotechnology.[2,3] Artificial enzymes have diverted extensive research efforts regarding their potential capabilities to dominate the natural enzyme's intrinsic limitations. Numerous nanomaterial-based artificial enzymes, also referred to as nanozymes, have peroxidase, oxidase, catalase, and superoxide dismutase mimic features and have wide application in biochemistry because of their benefits of low cost, easy fabrication, stability, and long-term storage.[4,5] These merits allow them to serve as promising materials in various fields, including biosystems control, *in vitro* implementation, and biomedical applications.

The extensive infectious disease outbreak caused by different pathogenic strains of bacteria and other microorganisms is one of the most serious health challenges worldwide and could result in fatal tissue lesions and chronic non-healing trauma. Several drugs have been detected to act as an initial defense system against pathogens by either inhibiting the proliferation or directly damaging the detrimental microorganisms.[6,7] Nevertheless, the risks of drug resistance, environmental pollution, complex chemical preparation, and expressivity have limited the extensive utilization of antibiotics.[8] Hence, recent investigations intend to discover novel alternative approaches, including antimicrobial photodynamic inactivation,[9] metal–organic semiconductors,[10] cations,[11] and artificial enzymes to obtain effective bacterial sterilization in low-dose usage of antibacterial elements. In particular, the peroxidase-like activity of nanozymes has drawn the most consideration for medical utilization in the case of antibacterial disinfection, which is associated with their reactive oxygen species (ROS), such as hydroxyl radical generation properties through the decomposition of hydrogen peroxide (H_2O_2).[12,13]

[a]*Department of Biology, Faculty of Natural Sciences, University of Tabriz, 51666-16471 Tabriz, Iran. E-mail: gdehghan@tabrizu.ac.ir*

[b]*Department of Applied Chemistry, Faculty of Chemistry, Research Laboratory of Advanced Water and Wastewater Treatment Processes, University of Tabriz, 51666-16471 Tabriz, Iran. E-mail: a_khataee@tabrizu.ac.ir*

[c]*Department of Chemical Engineering, Istanbul Technical University, 34469 Istanbul, Turkey*

[d]*Department of Basic Sciences, Division of Physiology, Faculty of Veterinary Medicine, Urmia University, 575615-1818, Urmia, Iran*

In recent years, several nanosized scaffolds including metal oxide nanoparticles,[14] nanofibers,[15] metal chalcogenides,[16] carbon nanotubes,[17] nanowires,[18] spinel ferrites,[19] metal–organic frameworks (MOF),[20,21] and layered double hydroxides (LDHs),[22] have been applied for use as natural peroxidase enzyme. Among the plentiful peroxidase mimic nanozymes, LDH-based hybrid or biohybrid substances, which are formed by positively charged brucite-like layers and interlamellar anions, have attained remarkable popularity to adopt in many processes owing to their great catalytic performances, simple synthesis, the flexibility of the compositions, and conformational stability. Structure formula of LDH is stated by $[M_{1-x}^{2+}M_x^{3+}(OH)_2]^{x+}[(A^{n-})_{x/n}, yH_2O]$ which M^{2+} and M^{3+} refer to divalent cations (Mg^{2+}, Ni^{2+}, Ca^{2+}, Cu^{2+}, Mn^{2+}, Co^{2+}, Ru^{2+}, Rh^{2+} or Zn^{2+}) and trivalent metal cations (Al^{3+}, Cr^{3+}, Ga^{3+}, Mn^{3+}, Co^{3+}, Ni^{3+} or Fe^{3+}), respectively. A^{n-} acts as an interlayer balancing anion that compensates the positive charge of the metal cations to recover the charge neutrality of LDH.[23] A number of studies have illustrated the capability of LDHs in photochemistry, separation technology, and medical applications such as different biomarker detection and drug carriers for cancer therapy.[24] The peroxidase-like activity of some LDHs, such as Co, Fe, and Ni has been reported as a novel property of LDHs.[25] The uniform distribution of metal ions and the large surface area of these two-dimensional inorganic solids make them suitable to act as nanozymes and to immobilize biomolecules to improve their efficiency in ROS generating.[26]

Despite the comprehensive investigations on the variety of nanomaterials in the case of enzyme imitating activity, their catalytic abilities are still inferior in comparison with natural enzymes due to the existence of confined sites on the surface of nanomaterials, which inevitably restrict their practical applications in disease diagnosis, potential bacterial control, virus detection, environmental treatment, biosensing, and nanomedicine.[27] In order to overcome the deficiencies of enzyme mimic nanomaterials, numerous strategies have been developed to simulate the natural enzymes' active site and improve the catalytic function of nanozymes.[22] Among these strategies, the most accurate sensing nanozymes could be obtained by decorating their surfaces with diverse functional compounds. To this day, different modifiers, including macromolecules, amino acids, DNA, and inorganic ions, have been utilized to improve the enzymatic properties of nanozymes.[28,29]

Naturally, the active site of enzymes has served as a vital catalytic center where the distribution of essential functional groups and amino acids follows a detailed spatial configuration. However, amino acids attract increasing attention based on their capabilities to simulate the catalytic active site of enzymes.[27] Some functional amino acids, such as histidine (His) in natural enzymes' active sites, act as Lewis acid–base and influence electron transition. His residue in the horseradish peroxidase (HRP) enzyme active site prepares an electronic local in natural enzymes active site to increase the production of hydroxyl radicals.[30,31] In addition, the distal histidine amino acid of HRP activates H_2O_2 molecules, binds them to the activated site's surface, and accelerates ROS production.[32] Herein, His provides the possibility of an effective catalytic performance through forming a hydrogen bond between the deprotonated N atom of its imidazole ring and the H atom of H_2O_2 thereby, the activation of H_2O_2. Therefore, introducing His on the nanoparticle surface increases the affinity for H_2O_2 as well as ROS production.[33]

However, the high pH of the bacterial systems inhibits the ROS production of nanozymes which commonly need an acidic condition.[34,35] Several studies have reported the ineffective production of ROS in an infected region with high pH.[36] An efficient technique is the design of nanozymes with high peroxidase activity in an acidic environment. In some reports, glucose oxidase (GOx) was utilized to produce gluconic acid to obtain an area with an acidic pH value. In these reports, the production of ROS and, consequently antibacterial efficacy was enhanced.[37,38] Nevertheless, a high concentration of nanozyme is still needed to successfully eliminate bacteria. As a result, it is a great issue to offer a highly efficient antibacterial nanozyme with high catalytic activity at a low dosage and acidic pH.

In this work, we comprehensively investigated the biological and nanozymatic potentials of His functionalized ZnCr-LDH nanoparticles as a new peroxidase-like platform inspired by the specific catalytic mechanism of the natural peroxidase. Zwitterionic L-His has an anionic carboxyl group and could be attached to positively charged layers of ZnCr LDH through electrostatic bonding. As expected, His could efficiently decorate the ZnCr-LDH with the co-existence of Zn and Cr ions due to the high specific surface area and rich redox reaction active sites of ZnCr-LDH, inducing a distinguished peroxidase mimic performance. Additionally, the strong peroxidase and antibacterial property of the His/ZnCr-LDH hybrid in the presence of GOx and glucose (Glu) was discovered as a feasible clinical approach against Gram-negative and Gram-positive bacteria and *in vivo* experiments, which have not been explored before. Moreover, the possible antimicrobial mechanism of the His/ZnCr-LDH hybrid was studied to meet the requirements of real-life applications.

2. Materials and methods

2.1. Chemicals

Zinc nitrate hexahydrate ($Zn(NO_3)_2 \cdot 6H_2O$), chromium(III) nitrate nonahydrate ($Cr(NO_3)_3 \cdot 9H_2O$), sodium hydroxide (NaOH), disodium phosphate (Na_2HPO_4), sodium acetate (NaAc)($C_2H_3NaO_2$), acetic acid (CH_3COOH), and yeast extract were provided from Merck (Germany). L-His ($C_6H_9N_3O_2$), 3,3′,5,5′-tetramethylbenzidine (TMB, $C_{16}H_{20}N_2$), Glu ($C_6H_{12}O_6$), GOx ($C_6H_{10}O_6$), glutaraldehyde ($C_5H_8O_2$), ethanol (C_2H_6O), hydrogen peroxide (H_2O_2), monosodium phosphate (NaH_2PO_4), sodium chloride (NaCl), propidium iodide (PI, $C_{27}H_{34}I_2N$) tryptone (C_3H_5NO), agar ($C_{14}H_{24}O_9$), and yeast extract were obtained from Sigma-Aldrich (USA). Ketamine hydrochloride and xylazine hydrochloride used to anesthetize rats were purchased from Alphasan (the Netherlands). Luria–Bertani medium was prepared by dissolving 0.5 g of yeast, 1 g of NaCl, and 1 g of tryptone in 100 mL of DI water. In addition, phosphate-buffered saline (PBS) was made by dissolving 8.475 g NaCl, 1.093 g Na_2HPO_4, and 0.276 g NaH_2PO_4 in 1 L DI water.

2.2. Fabrication of ZnCr-LDH and His/ZnCr-LDH

The LDH used in this study was prepared by the co-precipitation process. Briefly, 7.9 g of $Zn(NO_3)_2 \cdot 6H_2O$ and 4.6 g of $Cr(NO_3)_3 \cdot 9H_2O$ were dissolved in deionized water (DI). Then, NaOH solution (10^{-1} M) was added dropwise to the mentioned solution under the Ar atmosphere and stirred until it reached pH 9. The solution was stirred overnight at ambient temperature under an Ar atmosphere and the next day, the produced LDH was accumulated using a centrifuge and washed with DI water. Finally, precipitated LDH was dried in the oven at the temperature of 60 °C for 24 h.[39] To synthesize His/ZnCr LDH, a homogeneous suspension of ZnCr-LDH was prepared by dissolving 2 mg mL^{-1} of the LDH in DI and ultrasonication for 30 min. The obtained solution was mixed with His (500 μM, pH 8) with magnetic stirring for 24 h at ambient temperature. Zwitterionic L-His has an anionic carboxyl group and could be attached to positively charged layers of ZnCr LDH through electrostatic bonding. Then, the unbonded L-His was removed after centrifugation, and the His-modified ZnCr LDH (His/ZnCr LDH) precipitate was washed several times with DI water. Finally, the functionalized His/ZnCr LDH precipitate was dried.[40]

2.3. Characterization of nanomaterials

To determine the crystalline structure of the synthesized LDH and His/LDH, X-ray diffractometer (XRD) analysis Tongda, TD-3700 X-ray diffractometer system (Dandong, China) was applied. To assess the functional groups of the nanostructures, Fourier-transform infrared spectroscopy (FT-IR) analysis (Bruker, TENSOR 27 FT-IR, Germany) was utilized. Also, the morphological characteristics of the obtained nanostructures were evaluated using field effect scanning electron microscopy (FE-SEM) and EDX spectra analysis (MIRA3 FEG-SEM, Tescan, Czech Republic).

2.4. Catalytic activity of ZnCr-LDH and His/ZnCr-LDH

The peroxidase-like activity of the nanozymes was investigated *via* a colorimetric reaction using TMB as a chromogenic substrate. The nanostructure with peroxidase-like activity catalyzes the oxidation of TMB. It produces oxidized TMB in the proximity of H_2O_2 which has blue color, and a maximum absorbance peak at 652 nm and can be characterized by a UV-Vis spectrophotometer. For this purpose, the reaction solution containing nanostructure (400 μg mL^{-1}), TMB (0.2 mM), Glu (10–100 mM), and GOx (1 mg mL^{-1}) was mixed, and the UV-Vis absorption spectra were recorded at 625 nm after 5 min. In addition, the reaction of the nanostructures and TMB was studied, while the concentration of H_2O_2 was 300 μM. On the other hand, the enzyme-like activity of nanozymes is strongly influenced by pH, temperature, and substrate concentration. Therefore, the enzyme-like activity of His/ZnCr-LDH was measured at different pHs, temperatures, and concentrations of the substrates.

The enzymatic kinetic parameters of the LDH for H_2O_2 were analyzed in the detection solution containing acetate buffer (0.01 M, pH 5.0), His/ZnCr LDH (400 μg mL^{-1}), varying concentrations of H_2O_2 (50–500 μM), and a fixed concentration of TMB (0.2 mM). In another group, the kinetic parameter for TMB was obtained by changing the concentrations of TMB (26–280 μM) at a fixed concentration of H_2O_2 (500 μM) and the nanozyme (400 μg mL^{-1}), in acetate buffer (0.01 M, pH 5.0). For this purpose, the reactions were performed, and the absorbance changes of the reaction solution were studied at 652 nm. Finally, apparent kinetic parameters were estimated by fitting the obtained data to the Michaelis–Menten and Lineweaver–Burk plots and equations.[14]

2.5. Antibacterial activity of His/ZnCr-LDH

To investigate the antibacterial activity, bacteria suspensions were treated with various groups (Glu, Glu + GOx, GOx, His/ZnCr-LDH, His/ZnCr-LDH + Glu, His/ZnCr-LDH + GOx, ZnCr-LDH + Glu + GOx, and His/ZnCr-LDH + Glu + GOx) for 12 h and then, their optical density at 560 nm (OD_{560}) was recorded. Subsequently, to determine the minimum inhibitory concentration (MIC), bacteria suspension (*S. aureus* and *E. coli*, 10^6 CFU mL^{-1} in LB Broth solution) was incubated with different concentrations of His/ZnCr-LDH (2–8 μM) in the presence of GOx (1 mg mL^{-1}) and Glu (70 mM) at 37 °C overnight. After that, to enumerate the bacterial colonies, we made the agar plates by dissolving agar in LB Broth medium (0.015 g mL^{-1}) and then treated the bacteria with MIC concentrations and cultured them on the agar plates.

The morphological structure of treated *S. aureus* and *E. coli* suspension with His/ZnCr was tested by red fluorescence (PI) staining. For this purpose, *S. aureus* and *E. coli* suspension ($\sim 10^6$ CFU mL^{-1}) was treated with MIC concentration of His/ZnCr-LDH (3.5 μg mL^{-1} for *S. aureus* and 6 μg mL^{-1} for *E. coli*) in the presence of GOx (1 mg mL^{-1}) and Glu (70 mM) at 37 °C for 6 h. Then, the suspensions were centrifuged and washed with PBS 3 times. After that, the obtained bacteria were mixed with PI (2 μg mL^{-1}) and incubated at 37 °C for 20 min. Finally, the bacteria precipitations were collected by centrifuging and washing with PBS and investigated by fluorescence microscope.

In addition, the morphologies and membrane structures of treated and untreated bacteria samples were observed by SEM microscopy. In this regard, the bacteria were treated with His/LDH (3.5 μg mL^{-1} for *S. aureus* and 6 μg mL^{-1} for *E. coli*) at 37 °C for 4 h, and after that, the bacteria suspension was centrifuged. Then, PBS buffer was added to the bacteria precipitation, centrifuged, and fixed with 2.5% glutaraldehyde solution at 37 °C for 12 h. After that, the bacteria precipitate was dehydrated with 10, 30, 50, 70, 80, 90, and 100% ethanol solutions. Finally, the appearance and morphology of bacteria were observed and photographed with SEM microscope.

2.6. Disk diffusion method

Antibacterial activity of His/ZnCr-LDH in the presence of Glu and GOx was investigated against *S. aureus* and *E. coli* using the good diffusion method. For this purpose, we utilized LB-agar medium plates and then His/ZnCr-LDH + Glu + GOx containing disks were placed on the plates. After 24 h incubation, the

diameter of the growth inhibition zone of His/ZnCr-LDH was measured. A clean zone surrounding bacteria indicates that the antimicrobial treatment has effectively stopped or prevented microbial development.

2.7. Rat injury experiments

Twenty-four healthy adult male *Sprague Dawley* rats (190 ± 10 g, ~8 weeks of age) were provided from the animal house of the Laboratory of Physiology of Faculty of Veterinary Medicine of Urmia University and Veterinary Ethics Committee of the Faculty of Veterinary Medicine of Urmia University approved animal use procedures (IR-UU-AEC-3/1, 3/4/2023). The rats were randomized into four groups of 6 rats each according to the treatments and wound infections: (1) *E. coli* infected + PBS treated, (2) *E. coli* infected + His/ZnCr-LDH + Glu + GOx (20 μg mL^{-1}) treated, (3) *S. aureus* infected + PBS treated, and (4) *S. aureus* infected + His/ZnCr-LDH + Glu + GOx (20 μg mL^{-1}) treated. On the 0 days of experiments, rats were anesthetized using a cocktail of ketamine and xylazine (80 and 8 mg kg^{-1}, respectively). After shaving the backs of rats and aseptic preparation, a unilateral circular full-thickness cutaneous wound area was created by a sterile biopsy punch (6.0 mm diameter). The wounds of infected animal groups were soaked with 10 μL of the bacterial suspension (10^6 CFU mL^{-1}) and spread with a sterile swab to the wounds. From the first day, the mentioned solutions (PBS or His/ZnCr-LDH) dripped daily on the wound's surface. After that, the body weight and wound diameter in all rats were noted daily. The measuring tool of Adobe Acrobat 9 Pro Extended software (Adobe Systems Inc, San Jose, CA) was used to analyze the wound areas, and relative wound sizes (%) of the infected wound after, various treatments were calculated. Data collected from relative wound areas were analyzed using two-way ANOVA and Bonferroni's post hoc tests. GraphPad Prism 8.2.1 software (GraphPad Software, San Diego, CA, USA) was used for statistical analysis and a *P*-value less than 0.05 was considered significant.

3. Results and discussion

3.1. Characterization

Fig. 1A shows the FTIR spectra of the pure L-His, ZnCr-LDH, and His/ZnCr-LDH. This figure shows that pure L-His exhibits the characteristic vibrations of the OH, and C=O bands at 2852 cm^{-1}, and 1633 cm^{-1}, respectively.[41] In addition, N–H bending vibration and C–N stretching bands were observed at 1458 cm^{-1} and 1245 cm^{-1}, respectively. The pick around 3425 cm^{-1} is related to the NH_2 stretching vibrations of the amino acid.[41,42] In the spectra of ZnCr-LDH, the OH stretching vibrations of the basal OH groups and interlayer water were observed at 3100–3600 cm^{-1}. The characteristic ν_3 and ν_2 vibration modes of compensating NO_3^- interlayer anions were observed at 1382 cm^{-1} and 833 cm^{-1}.[43] On the other hand, the characteristic absorption peaks at 567 cm^{-1} and 505 cm^{-1} are assigned to the Zn–O and Cr–O stretching modes, respectively.[44] The observed spectral changes in the FTIR spectrum of His/ZnCr-LDH confirmed the successful modification of ZnCr-LDH by L-His. The decrease of the OH vibration, N–H bending vibration, C=O vibration, and C–N stretching of His after immobilization on ZnCr-LDH point to the condensation reaction and the formation of amide bonds.

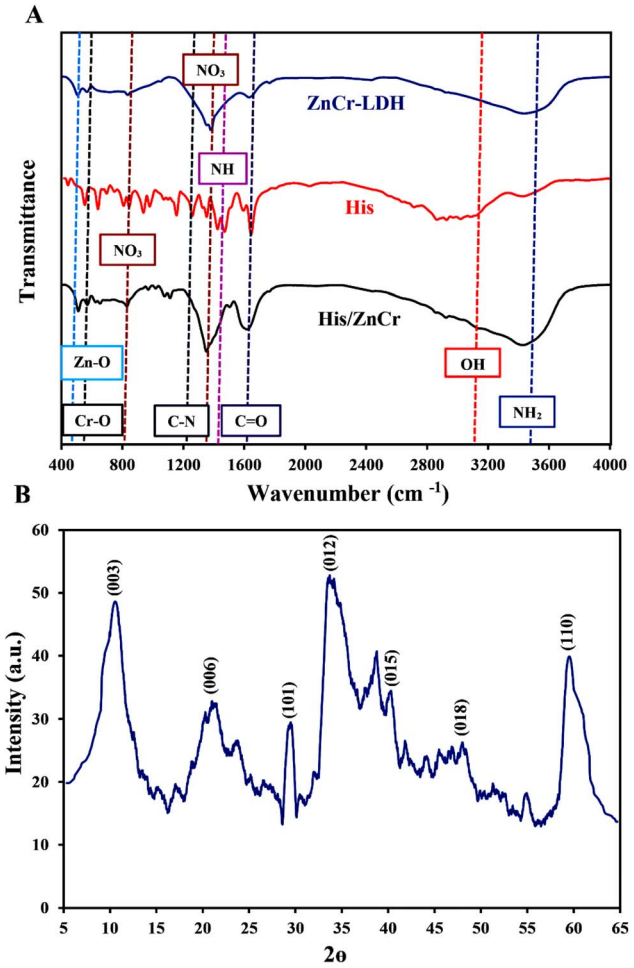

Fig. 1 Characterization of fabricated nanostructures: (A) FTIR spectrum of ZnCr-LDH, His, and His/ZnCr-LD; (B) XRD pattern of ZnCr-LDH.

The XRD pattern of the fabricated ZnCr-LDH is given in Fig. 1B. According to our previous study (JCPDS standard card 51-1525),[45] the sharp diffraction peaks that are located at about 10°, 20°, 32.5°, 34°, 39.5°, 48.5°, and 60.6° can be indexed to the 003, 006, 101, 012, 015, 018, and 110 crystalline planes of ZnCr-LDH.

The morphology of ZnCr-LDH and His/ZnCr-LDH was investigated by the FE-SEM method and the obtained results are presented in Fig. 2. ZnCr-LDH displays a stacked disk-like shape with submicron size (Fig. 2A–C). As shown in these images, the ZnCr-LDHs have a plate-like structure assembled by the side-face contacted ultra-fine LDH nanosheets.[46] In addition, His and modified ZnCr-LDH SEM images were shown in Fig. 2D–F. As depicted in Fig. 2D and reported in previous studies, His amino acids have a crystalline morphology[47] and were detected on the surface of the modified ZnCr-LDH (Fig. 2E and F). These

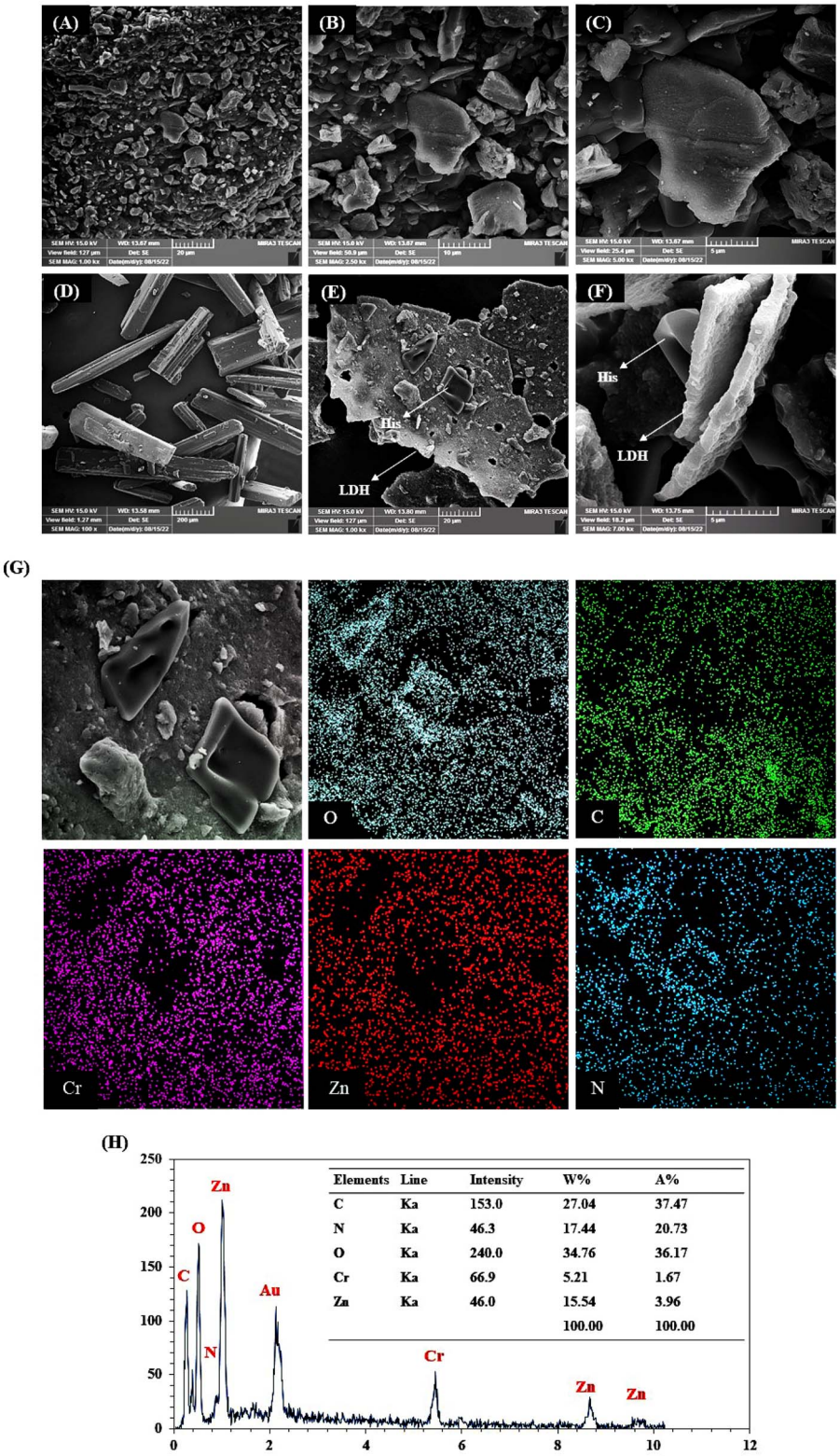

Fig. 2 FE-SEM images: (A–C) ZnCr-LDH; (D) His, (E and F) His/ZnCr-LDH; (G) elemental mapping of C, N, O, Zn, and Cr; and (H) EDX pattern and elemental weight percent of His/ZnCr-LDH.

images show the attachment of the crystal-like structure of His to the nanosheet structure of the LDHs in His/ZnCr-LDH.

Fig. 2G depicts the elemental mapping analysis of ZnCr-LDH after modification. In the mapping images of His/ZnCr-LDH, in addition to the nanoparticle elements, C and N were also

observed, which were related to the His amino acids. On the other hand, the EDX spectrum and elemental weight percent of His/ZnCr-LDH are shown in Fig. 2H. As expected, EDX analysis for His/LDH shows the presence of the nanoparticle elements (Zn and Cr) and histidine elements (N, O, C), which confirms the modification of the LDH.

3.2. Peroxidase-mimic activity of His/ZnCr-LDH

The enzyme-like activity of His/ZnCr-LDH was tested using a TMB oxidation-based colorimetric method in the presence of H_2O_2 and recording the absorption peak at 652 nm. By catalytically oxidizing Glu with GOx enzyme, which was added to the reaction solution, the required H_2O_2 was generated *in situ*. Then, the produced H_2O_2 was catalyzed by His/ZnCr-LDH and released free radicals, reacting with TMB to produce ox-TMB. The findings revealed that colorless TMB can be oxidized in the presence of His/ZnCr-LDH, GOx, and Glu, producing a blue-colored ox-TMB with maximum absorption at 652 nm (Fig. 3A). In control experiments, His and ZnCr-LDH were used as catalysts to investigate their peroxidase-mimic activity alone (Fig. 3B–D). The mixture of His or ZnCr-LDH with Glu and GOx showed no significant peroxidase-like activity. In contrast, a considerable amount of catalytic activity was observed after the modification of ZnCr-LDH with His (His/ZnCr-LDH). These results proved that the binding of His on the surface of the LDH increases the production of free radicals and, thus the oxidation of TMB.[48]

In addition, the optimum concentration of Glu for the peroxidase-like activity of the prepared catalyst was estimated to be 70 μM, and the reaction rate reaches a plateau at high substrate concentrations (higher than 70 μM), which is due to the saturation of active sites on GOx with substrate and the reduction of the generation of H_2O_2 at high Glu concentrations.

On the other hand, the generation of gluconic acid (GA), the other product of the oxidation of Glu through the GOx enzyme activity, was evaluated by recording the alterations in pH during the reaction time. As expected according to previous reports,[12] the *in situ* pH value gradually decreased to about 4.0, confirming the production of GA (Fig. 3E). Therefore, the peroxidase-like activity of His/ZnCr-LDH was investigated at pH 4 and different pH values. Since His/ZnCr-LDH can oxidize TMB and cause an obvious absorption change, the absorbance of the reaction solution in the presence of H_2O_2 at 652 nm was recorded during the catalytic reaction to investigate the catalytic activity of the modified LDH at different pHs. As shown in Fig. 3F, with decreasing pH values (up to 4), TMB oxidation

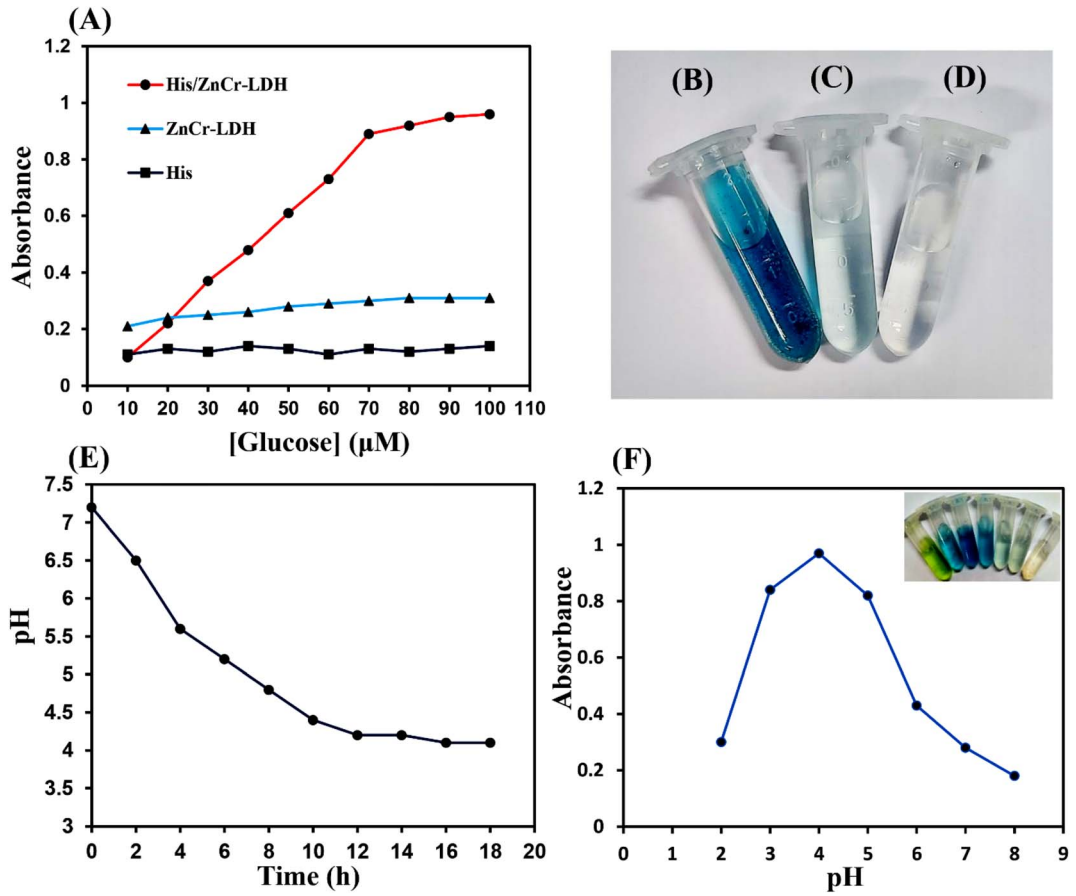

Fig. 3 (A) The peroxidase-mimic activity of ZnCr-LDH, His, and His/ZnCr-LDH in the presence of GOx and different concentrations of Glu; (B–D) oxidation of TMB by His/ZnCr-LDH, ZnCr-LDH, and His; (E) change of pH value during the reaction of GOx with Glu; (F) effect of pH change on peroxidase-like activity of His/ZnCr-LDH.

increased, and when the pH value reached 4, the highest reaction rate was observed. Also, the enzyme-mimic activity of His/ZnCr-LDH was tested after incubation at different temperatures (from 15 to 50 °C). The results illustrated that the His/ZnCr-LDH has high catalytic activity at 20–30 °C. These results revealed that the peroxidase-mimic activity of His/ZnCr-LDH is strongly dependent on pH and temperature. It has been reported that small and monodispersed particles can be produced under the optimum conditions of temperature and pH. The generation of small particles enhances the surface/volume ratio, which can increase the catalytic activity.[49]

The reaction kinetic parameters were obtained using various concentrations of TMB and H_2O_2 as substrates. The obtained results indicated that the initial reaction rate increased with increasing H_2O_2 and TMB concentrations. However, the reaction rate reached its maximum at higher substrate concentrations, which was due to the active site saturation on the surface of His/ZnCr-LDH (like natural enzymes).[50] The Lineweaver–Burk curves of peroxidase-mimic His/ZnCr-LDH were plotted (Fig. 4A and B) and the kinetic parameters were calculated (Table 1). The K_m values (an indicator of enzyme affinity towards its substrate) for the His/ZnCr-LDH with TMB and H_2O_2 were 0.27 and 1.55 mM, respectively. Compared to horseradish peroxidase (HRP), the K_m values of peroxidase-mimic His/ZnCr-LDH were low for both substrates, indicating the highest affinity of the prepared particles for TMB and H_2O_2.

Table 1 Calculated kinetic parameters for peroxidase-mimic His/ZnCr-LDH

Catalyst	Substrate	K_m (mM)	Ref.
HRP	TMB	0.43	51
	H_2O_2	3.7	51
His/ZnCr-LDH	TMB	0.27	This work
	H_2O_2	1.55	This work

3.3. Antibacterial investigation of His/ZnCr-LDH

3.3.1. *In vitro* antibacterial activity. To determine the antibacterial activity of LDH, the absorbance (OD560) of *S. aureus* and *E. coli* liquid medium containing His/ZnCr-LDH with or without Glu, and GOx was measured under the same conditions. As is shown in Fig. 5A and B, when the concentration of the nanostructure was 4 μg mL^{-1}, in the absence of Glu and GOx *S. aureus* and *E. coli* samples only exhibited inhibition rates of 21.42% and 14.28%, respectively. The inhibition rates were 90.62% and 84.61% in the presence of Glu and GOx for *S. aureus* and *E. coli*, respectively. Similar to the previous findings, this result also confirmed that the presented nanozyme has higher activity in acidic conditions resulting from GOx enzyme activity and produces more radicals using the generating H_2O_2.

To measure the minimal inhibition concentrations (MIC) of His/LDH in the presence of Glu and GOx in *S. aureus* and *E. coli*, we treated the bacteria with Glu, GOx, and different concentrations of His/LDH (Fig. 5C and D). When the concentration of the LDH reached 3.5 μg mL^{-1}, the OD_{560} of media containing *S. aureus* was the same as the group that contained only LB broth (Fig. 5C). Similarly, the MIC for His/LDH accompanied by Glu and GOx for *E. coli* is estimated to be 6 μg mL^{-1} (Fig. 5D). The obtained MIC values were similar or even better than other similar works[12] and indicated that the antibacterial activity of the presented nanozyme was higher against *S. aureus* than *E. coli*.

Propidium iodide (PI) staining was carried out to confirm the destruction of bacterial membranes. Through PI staining, fluorescence microscopy was used to recognize membrane-compromised treated bacteria with His/LDH. The unscathed membrane is impenetrable for PI with red fluorescence, while damage to the bacterial membrane allows the dye to penetrate the bacteria. So, different fluorescence signals can detect the destruction of bacterial membranes. As can be seen in Fig. 5E, when *S. aureus* and *E. coli* suspensions were incubated with His/ZnCr-LDH in the presence of Glu and GOx, fluorescence images show increased red fluorescence spots, indicating that His/ZnCr-LDH can lead to bacteria membrane disruption. The increase in the number of red fluorescence spots in the presence of the LDH indicates the production and attack of ROS toward the bacterial membrane.[52]

3.3.2. Disc diffusion assay. Antibacterial activity of the His/ZnCr-LDH was evaluated against *S. aureus* and *E. coli* by the good diffusion method (Fig. 6A). As shown in the figure, His/ZnCr-LDH in the presence of GOx and Glu was able to inhibit

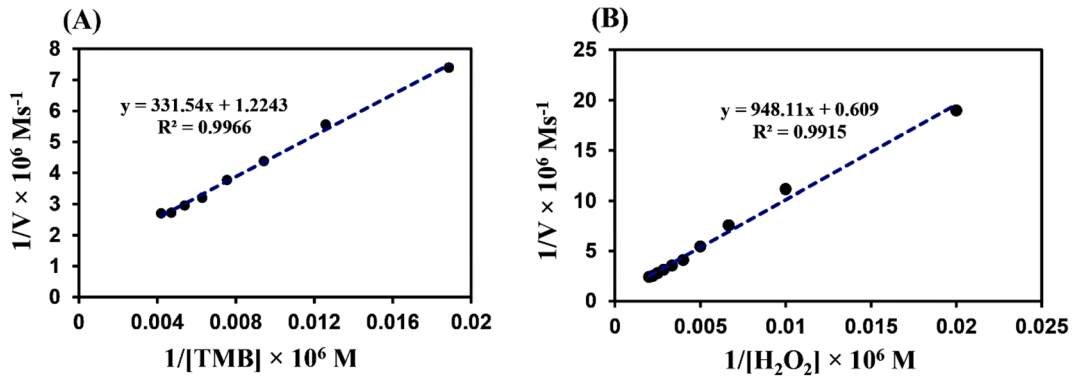

Fig. 4 Steady-state kinetic assays of His/ZnCr-LDH: (A) for TMB and (B) H_2O_2.

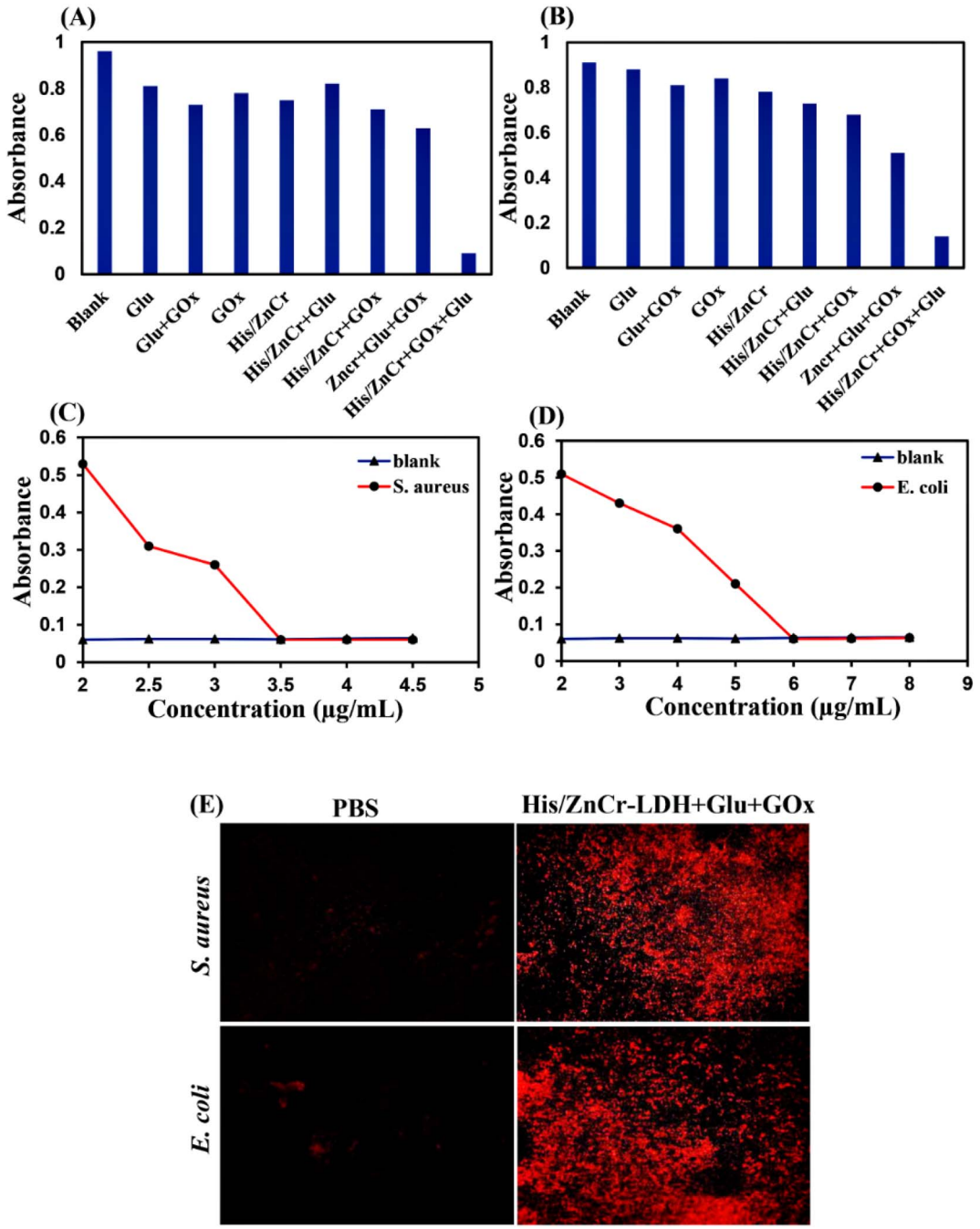

Fig. 5 Antibacterial tests: (A) the OD560 of *S. aureus* and (B) *E. coli* liquid medium treated with Glu, Glu + GOx, GOx, His/ZnCr, His/ZnCr + Glu, His/ZnCr + GOx, ZnCr + Glu + GOx, and His/ZnCr + Glu + GOx; (C) the OD_{560} of *S. aureus* and (D) *E. coli* liquid medium treated with different concentrations of His/ZnCr in the presence of Glu and GOx; (E) fluorescence microscopy images of *S. aureus* and *E. coli* treated with PBS and His/ZnCr + Glu + GOx.

bacterial growth. The zone of inhibition around the discs was measured to be 3 cm (for *S. aureus*) and 2 cm (for *E. coli*). According to the previous results, this data showed that Gram-positive *S. aureus* is more sensitive to free radicals than Gram-negative *E. coli*. In addition, control experiments were carried out using GOx, Glu, Glu + GOx, His, ZnCr-LDH, and His/ZnCr-LDH alone, and the findings revealed no inhibition zone. So, as expected, none of the mentioned agents could produce acceptable amounts of free radicals and, therefore destroy bacteria. These results confirmed that bacterial growth suppression was due to the production of H_2O_2 *in situ* through the GOx reaction, which catalyzes the oxidation of Glu and the production of GA and H_2O_2. Then, the peroxidase-mimic His/ZnCr-LDH oxidizes H_2O_2 during the GOx reaction and produces free radicals, and the free radicals produced can inhibit bacterial growth.

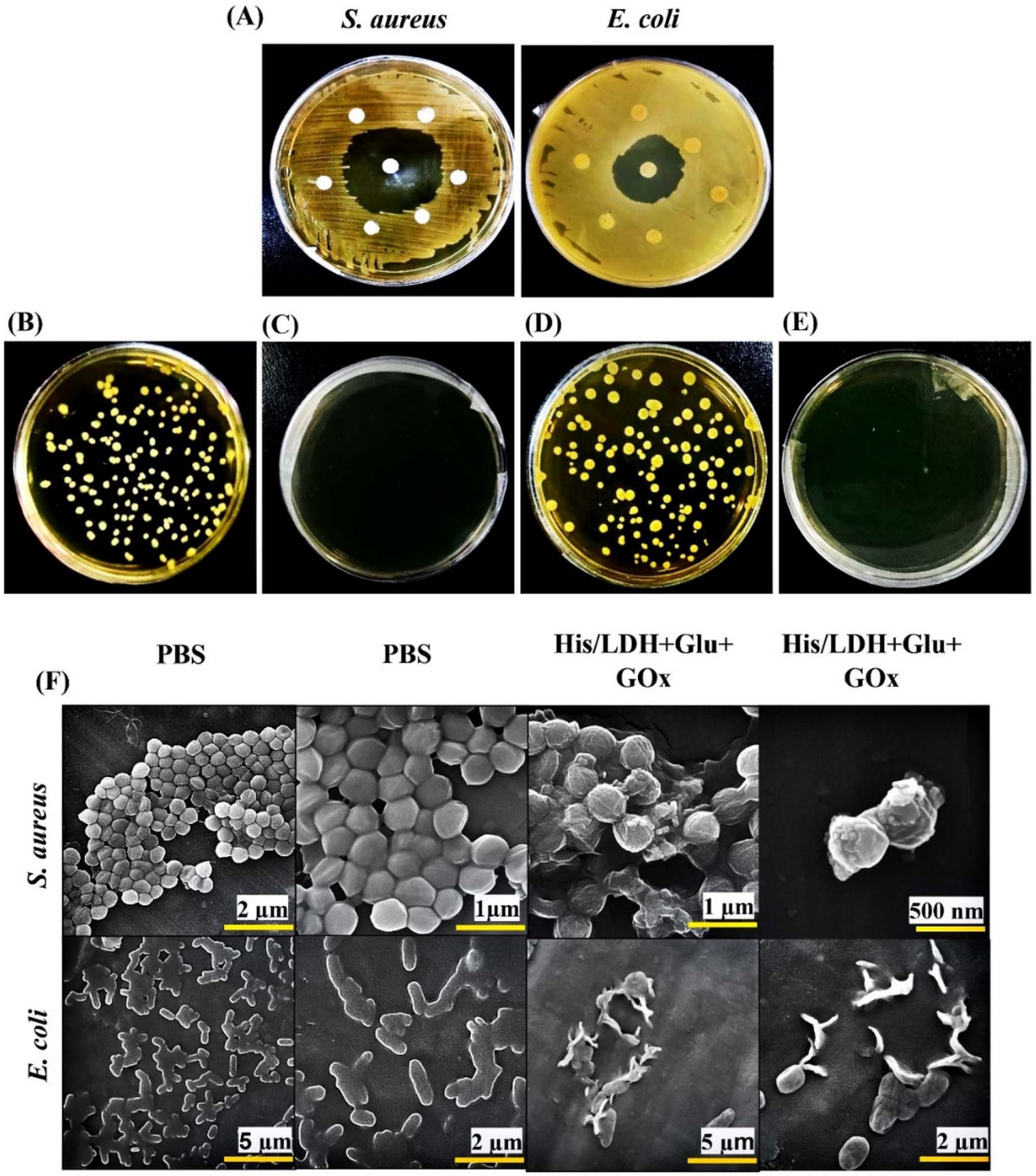

Fig. 6 Antibacterial tests: (A) disc diffusion assay against *S. aureus* and *E. coli*; (B and C) solid agar plate images of *S. aureus* treated with PBS and His/ZnCr-LDH + Glu + GOx, (D and E) solid agar plate images of *E. coli* treated with PBS and His/ZnCr-LDH + Glu + GOx (F) SEM images of *S. aureus* and *E. coli* treated with PBS and His/ZnCr-LDH + Glu + GOx.

Furthermore, bacterial samples (untreated and treated with MIC concentration of His/ZnCr-LDH) were diluted and sprayed on solid agar plates. The results indicated that the control plates had a higher density of bacterial colonies (Fig. 6B and D). However, the samples treated with His/ZnCr-LDH + Glu + GOx depicted no bacterial colonies (Fig. 6C and E). These results agree with the previous outcomes obtained in the present work.

3.3.3. Determination of bacterial morphology. The bacterial morphology was investigated using FE-SEM analysis of *S. aureus* and *E. coli* and after 4 h treatment with His/ZnCr-LDH. The untreated bacterial cells were considered as control. Fig. 6F depicts the bacteria without and with the addition of His/ZnCr-LDH. According to this figure, a normal morphology was observed for the untreated bacterial cells. However, it is clear that treated samples showed damaged shapes, and the bacterial cells lost their membrane integrity.[53,54] These results indicated the formation of free radicals through the peroxidase-mimic activity of His/ZnCr-LDH, which damages the bacterial cell membrane. It has been reported that free radicals damage cell membranes by reacting directly with polyunsaturated fatty acids in membranes and initiating lipid peroxidation.[55]

3.3.4. Rat injury experiments. Fig. 7 displays a schematic illustration of the antibacterial performance in the rat incision wound model (A), the wound healing process photos at different

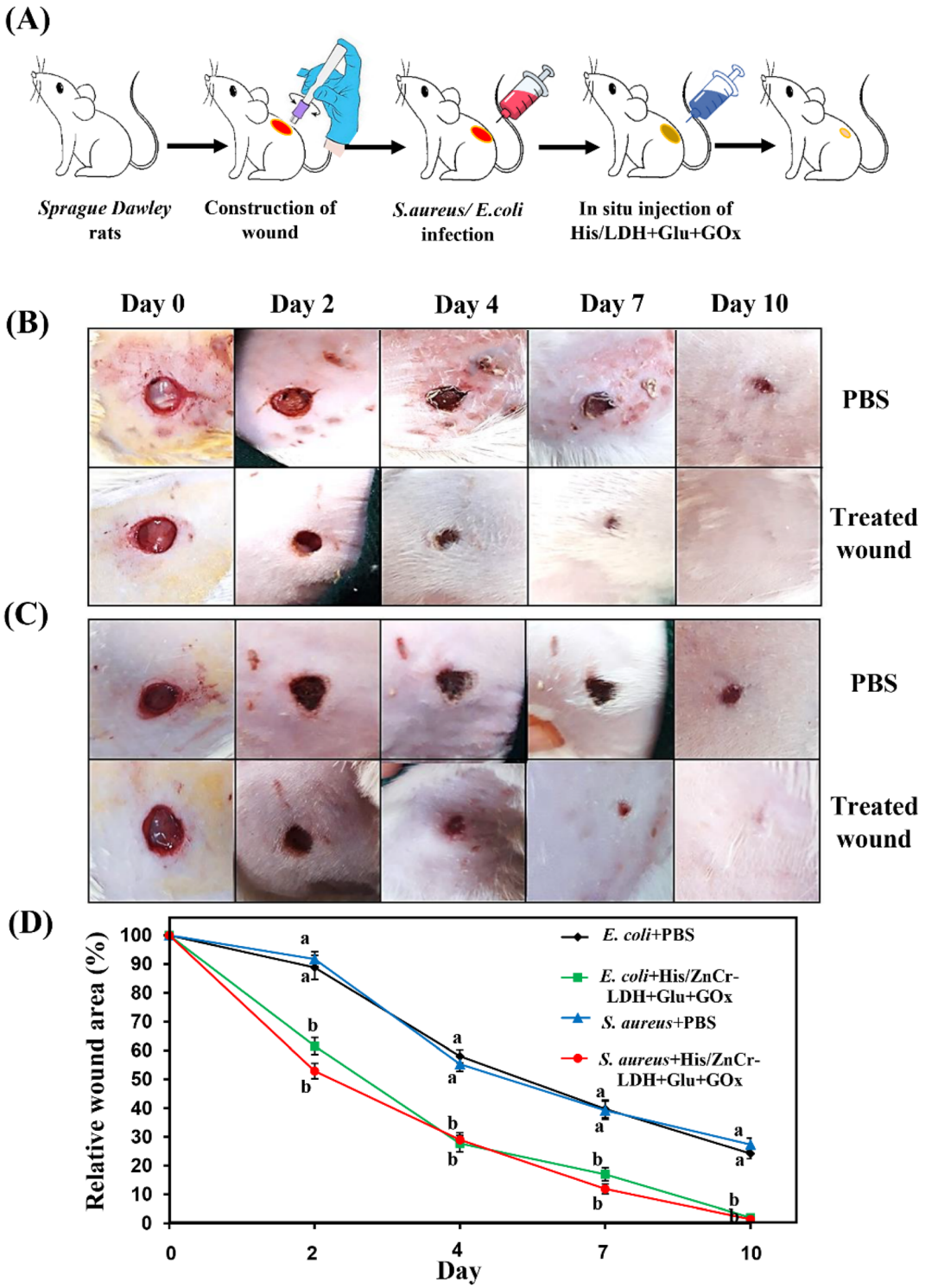

Fig. 7 *In vivo* antibacterial test: (A) schematic image of the *in vivo* antibacterial activity of His/ZnCr-LDH; (B) photographs of wound areas infected by *S. aureus* and (C) *E. coli* after therapies on days 0, 2, 4, 7, and day 10; (D) relative wound areas (%) of the infected wound after different treatments on day 0, day 2, day 4, day 7, and 10; in (D), different letters represent significant differences ($P < 0.001$) compared to corresponding time points using two-way ANOVA and Bonferroni post hoc tests. All values are expressed as the mean ± SEM.

time intervals (B and C), and percentages of wound area reduction in different time points (D) across all the experimental groups. The *S. aureus* + His/LDH + Glu + GOx, and *E. coli* + His/LDH + Glu + GOx treated groups showed a faster wound healing process (complete healing after 10 days from wound induction). The relative wound area was significantly lower ($P < 0.001$) in *S. aureus* + His/LDH + Glu + GOx treated group compared to the *S. aureus* + PBS at day 2, day 4, day 7, and 10. In

addition, the relative wound area of the *E. coli* + His/LDH + Glu + GOx treated group was significantly ($P < 0.001$) lower than the *E. coli* + PBS at the above-mentioned intervals.

4. Conclusion

In summary, in the present work, we developed a novel acid-enhanced antibacterial platform using the high peroxidase-like activity and excellent ROS generation ability of His-functionalized ZnCr-LDH. The generated hydroxyl radicals from H_2O_2, produced by the GOx enzyme, may damage the bacterial membranes and thus lead to the elimination of the bacteria. It is very important to note that the other production of GOx catalytic reaction, GA, effectively reduces the pH level of the infected area, which can increase the peroxidase-mimic activity, production of ROS, and the ability of His/ZnCr-LDH to eradicate bacteria at a very low concentration. The application of the antibacterial ability of His/ZnCr-LDH nanozyme was assessed in rat injury experiments. *In vivo* tests confirmed that His/ZnCr-LDH could accelerate the disinfection and curing of infected wounds. Due to the presence of Glu in the presented method, the strategy can be an appropriate option for treating diabetic ulcer wounds.

Conflicts of interest

There are no conflicts to declare.

Acknowledgements

The authors wish to thank the University of Tabriz for the support.

References

1 Y. R. Maghraby, R. M. El-Shabasy, A. H. Ibrahim and H. M. E.-S. Azzazy, *ACS Omega*, 2023, **8**, 5184–5196.
2 N. G. Nezhad, R. N. Z. R. Abd Rahman, N. M. Yahaya, S. N. Oslan, F. M. Shariff and T. C. Leow, *Int. J. Biol. Macromol.*, 2023, 123440.
3 L. Alvarado-Ramírez, M. Rostro-Alanis, J. Rodríguez-Rodríguez, J. E. Sosa-Hernández, E. M. Melchor-Martínez, H. M. Iqbal and R. Parra-Saldívar, *Biosensors*, 2021, **11**, 410.
4 S. Wang, W. Deng, L. Yang, Y. Tan, Q. Xie and S. Yao, *ACS Appl. Mater. Interfaces*, 2017, **9**, 24440–24445.
5 Z. Wang, K. Dong, Z. Liu, Y. Zhang, Z. Chen, H. Sun, J. Ren and X. Qu, *Biomaterials*, 2017, **113**, 145–157.
6 T. Khan, K. Sankhe, V. Suvarna, A. Sherje, K. Patel and B. Dravyakar, *Biomed. Pharmacother.*, 2018, **103**, 923–938.
7 M. A. Kohanski, D. J. Dwyer, B. Hayete, C. A. Lawrence and J. J. Collins, *Cell*, 2007, **130**, 797–810.
8 S. A. Kraemer, A. Ramachandran and G. G. Perron, *Microorganisms*, 2019, **7**, 180.
9 J. Li, S. Song, J. Meng, L. Tan, X. Liu, Y. Zheng, Z. Li, K. W. K. Yeung, Z. Cui and Y. Liang, *J. Am. Chem. Soc.*, 2021, **143**, 15427–15439.
10 Z. M. Davoudi, A. E. Kandjani, A. I. Bhatt, I. L. Kyratzis, A. P. O'Mullane and V. Bansal, *Adv. Funct. Mater.*, 2014, **24**, 1047–1053.
11 X. Huang, L. Tian, Z. Wang, J. Zhang, Y. S. Chan, S. H. Cheng and X. Yao, *Adv. Funct. Mater.*, 2020, **30**, 2004166.
12 M. Wang, X. Zhou, Y. Li, Y. Dong, J. Meng, S. Zhang, L. Xia, Z. He, L. Ren and Z. Chen, *Bioact. Mater.*, 2022, **17**, 289–299.
13 B. Oskouei, G. Dehghan, M. Mahdavi and M. A. H. Feizi, *Appl. Clay Sci.*, 2023, **237**, 106914.
14 S. Rashtbari, G. Dehghan, M. Amini, S. Khorram and A. Khataee, *Chemosphere*, 2022, **295**, 133747.
15 C. Zhang, X. Xue, Q. Luo, Y. Li, K. Yang, X. Zhuang, Y. Jiang, J. Zhang, J. Liu and G. Zou, *ACS Nano*, 2014, **8**, 11715–11723.
16 W. He, H. Jia, X. Li, Y. Lei, J. Li, H. Zhao, L. Mi, L. Zhang and Z. Zheng, *Nanoscale*, 2012, **4**, 3501–3506.
17 Q. Zhang, X. He, A. Han, Q. Tu, G. Fang, J. Liu, S. Wang and H. Li, *Nanoscale*, 2016, **8**, 16851–16856.
18 Y. Wang, C. Chen, D. Zhang and J. Wang, *Appl. Catal., B*, 2020, **261**, 118256.
19 Z. Yang, Y. Zhu, M. Chi, C. Wang, Y. Wei and X. Lu, *J. Colloid Interface Sci.*, 2018, **511**, 383–391.
20 J. Wu, F. Xu, S. Li, P. Ma, X. Zhang, Q. Liu, R. Fu and D. Wu, *Adv. Mater.*, 2019, **31**, 1802922.
21 X. Liu, Q. Deng, L. Zhang, Y. Sang, K. Dong, J. Ren and X. Qu, *Chem. Commun.*, 2021, **57**, 2903–2906.
22 S. Dadakhani, G. Dehghan and A. Khataee, *Spectrochim. Acta, Part A*, 2023, 123016.
23 M. Sajid and C. Basheer, *TrAC, Trends Anal. Chem.*, 2016, **75**, 174–182.
24 D. Tonelli, E. Scavetta and M. Giorgetti, *Anal. Bioanal. Chem.*, 2013, **405**, 603–614.
25 W. Yang, J. Li, M. Wang, X. Sun, Y. Liu, J. Yang and D. H. Ng, *Colloids Surf., B*, 2020, **188**, 110742.
26 M. Asif, A. Aziz, M. Azeem, Z. Wang, G. Ashraf, F. Xiao, X. Chen and H. Liu, *Adv. Colloid Interface Sci.*, 2018, **262**, 21–38.
27 K. Fan, H. Wang, J. Xi, Q. Liu, X. Meng, D. Duan, L. Gao and X. Yan, *Chem. Commun.*, 2017, **53**, 424–427.
28 W. Zhang, X. Niu, S. Meng, X. Li, Y. He, J. Pan, F. Qiu, H. Zhao and M. Lan, *Sens. Actuators, B*, 2018, **273**, 400–407.
29 S. Rashtbari and G. Dehghan, *J. Hazard. Mater.*, 2021, **406**, 124340.
30 M. Sha, W. Xu, Y. Wu, L. Jiao, Y. Chen, J. Huang, Y. Tang, W. Gu and C. Zhu, *Sens. Actuators, B*, 2022, **366**, 131927.
31 R. Khodarahmi, M. R. Ashrafi-Kooshk, S. Khodarahmi, S. A. Ghadami and A. Mostafaie, *Int. J. Biol. Macromol.*, 2015, **80**, 293–301.
32 Y.-C. Yang, Y.-T. Wang and W.-L. Tseng, *ACS Appl. Mater. Interfaces*, 2017, **9**, 10069–10077.
33 L. Zhang, Z. Huang, Y. Han, Z. Guo, X. Zhang, R. Xie and W. Yang, *Appl. Surf. Sci.*, 2020, **532**, 147457.
34 X. d. Wang, R. J. Meier and O. S. Wolfbeis, *Angew. Chem., Int. Ed.*, 2013, **52**, 406–409.
35 X. Xie, T. Sun, J. Xue, Z. Miao, X. Yan, W. Fang, Q. Li, R. Tang, Y. Lu and L. Tang, *Adv. Funct. Mater.*, 2020, **30**, 2000511.
36 Q. Mu, Y. Sun, A. Guo, X. Xu, B. Qin and A. Cai, *J. Hazard. Mater.*, 2021, **402**, 123939.

37 X. Liu, Z. Yan, Y. Zhang, Z. Liu, Y. Sun, J. Ren and X. Qu, *ACS Nano*, 2019, **13**, 5222–5230.
38 X. Cheng, S. Zhang, H. Liu, H. Chen, J. Zhou, Z. Chen, X. Zhou, Z. Xie, Q. Kuang and L. Zheng, *ACS Appl. Mater. Interfaces*, 2020, **12**, 36996–37005.
39 T. S. Rad, A. Khataee, S. Arefi-Oskoui, S. S. Rad, Y. Orooji, E. Gengec and M. Kobya, *Chemosphere*, 2022, **286**, 131740.
40 M. Shamsayei, Y. Yamini and H. Asiabi, *Colloid Interface Sci.*, 2018, **529**, 255–264.
41 S. Rat, A. Chavez-Sanchez, M. Jerigová, D. Cruz and M. Antonietti, *ACS Appl. Polym. Mater.*, 2021, **3**, 2588–2597.
42 M. Tsoeunyane, M. Makhatha and O. Arotiba, *Int. J. Corros.*, 2019, **2019**, 7406409.
43 S. D. Bencherif, J. J. Gallardo, I. Carrillo-Berdugo, A. Bahmani and J. Navas, *Nanomater*, 2021, **11**, 3051.
44 M. Dinari, M. M. Momeni and Y. Ghayeb, *J. Mater. Sci.: Mater. Electron.*, 2016, **27**, 9861–9869.
45 T. S. Rad, A. Khataee, S. S. Rad, S. Arefi-Oskoui, E. Gengec, M. Kobya and Y. Yoon, *Ultrason. Sonochem.*, 2022, **82**, 105875.
46 J. Lin, Y. Zhang, Q. Zhang, J. Shang and F. Deng, *Environ. Sci. Pollut. Res.*, 2021, **28**(35), 48236–48252.
47 T. Menahem and Y. Mastai, *J. Polym. Sci., Part A: Polym. Chem.*, 2006, **44**, 3009–3017.
48 S. Ponnusamy, L. Sandhiya and K. Senthilkumar, *New J. Chem.*, 2017, **41**, 10259–10271.
49 S. Rashtbari, G. Dehghan, S. Khataee, M. Amini and A. Khataee, *Chemosphere*, 2022, **291**, 133063.
50 X. Han, R. Liu, H. Zhang, Q. Zhou, W. Feng and K. Hu, *Chem.–Asian J.*, 2021, **16**, 1603–1607.
51 W. Chen, J. Chen, A. L. Liu, L. M. Wang, G. W. Li and X. H. Lin, *ChemCatChem*, 2011, **3**, 1151–1154.
52 F. Wei, X. Cui, Z. Wang, C. Dong, J. Li and X. Han, *J. Chem. Eng.*, 2021, **408**, 127240.
53 S. K. Verma, E. Jha, B. Sahoo, P. K. Panda, A. Thirumurugan, S. Parashar and M. Suar, *RSC Adv.*, 2017, **7**, 40034–40045.
54 V. Gopinath, S. Priyadarshini, M. F. Loke, J. Arunkumar, E. Marsili, D. MubarakAli, P. Velusamy and J. Vadivelu, *Arabian J. Chem.*, 2017, **10**, 1107–1117.
55 Y. Hong, J. Zeng, X. Wang, K. Drlica and X. Zhao, *Proc. Natl. Acad. Sci.*, 2019, **116**, 10064–10071.